Static Bell test in pilot-wave hydrodynamics

Konstantinos Papatryfonos, Louis Vervoort, André Nachbin, Matthieu Labousse, John W M Bush

Static Bell test in pilot-wave hydrodynamics

Konstantinos Papatryfonos
Gulliver, CNRS, ESPCI Paris, Université PSL,
10 rue Vauquelin, 75005 Paris, France and
Department of Mathematics, MIT, 77 Massachusetts Ave., Cambridge MA 02139, USA[*]

Louis Vervoort
Higher School of Economics, 101000 Moscow, Russian Federation[†]

André Nachbin[‡]
Department of Mathematical Sciences, WPI,
100 Institute Road, Worcester MA 01609, USA

Matthieu Labousse[§]
Gulliver, CNRS, ESPCI Paris, Université PSL, 10 rue Vauquelin, 75005 Paris, France

John W. M. Bush[¶]
Department of Mathematics, MIT, 77 Massachusetts Ave., Cambridge MA 02139, USA[*]

(Dated: October 2, 2024)

Since its discovery in 2005, the hydrodynamic pilot-wave system has provided a concrete macroscopic realization of wave-particle duality and concomitant classical analogs of a growing number of quantum effects. The question naturally arises as to how closely particle-particle correlations achieved with this classical system can mimic those arising on the quantum scale. We here introduce a new platform for addressing this question, a numerical model of cooperative tunneling in a bipartite pilot-wave hydrodynamic system. We execute a static Bell test, in which the system geometry is fixed and the two subsystems are coupled through the intervening wave field. This wave-mediated coupling is not congruent with the assumptions made in deriving Bell's inequality, and so allows one to rationalize the reported violations. Nevertheless, these violations are elusive, and arise only in a limited corner of parameter space.

[*] kpapatry@mit.edu
[†] lvervoort@hse.ru
[‡] anachbin@wpi.edu
[§] matthieu.labousse@espci.psl.eu
[¶] bush@math.mit.edu

I. INTRODUCTION

In 2005, Yves Couder and Emmanuel Fort [1, 2] discovered that a millimetric droplet may self-propel along the surface of a vibrating fluid bath through a resonant interaction with its own wave field. The resulting 'walker' consists of a droplet dressed in a quasi-monochromatic wave field, and represents a concrete, macroscopic example of wave-particle duality [3]. Remarkably, this hydrodynamic pilot-wave system exhibits many features previously thought to be exclusive to the microscopic, quantum realm [4, 5]. Notable examples include single-particle diffraction and interference [2, 6, 7], quantized orbits [3, 8], unpredictable tunneling [9], Friedel oscillations [10], surreal trajectories [11], spin lattices [12], and quantum-like statistics and statistical projection effects in corrals [13, 14]. In all instances, the emergent quantum behavior may be rationalized in terms of the droplet's non-Markovian pilot-wave dynamics [5]. Specifically, the instantaneous wave force imparted to the drop during impact depends on the droplet's history. Thus, the drop navigates a potential landscape of its own making [5], and the hydrodynamic pilot-wave system is said to be endowed with 'memory' [15]. The walking-droplet system has provided a framework for exploring the boundary between classical and quantum behavior. Moreover, it has inspired investigations of other hydrodynamic pilot-wave systems in which oscillators interact with their suspending fluids [16–19].

In several settings, long-range interactions in the walking-droplet system arise through the influence of the pilot-wave field [5]. For example, long-range lift forces are generated when a walking droplet interacts with a submerged pillar [20] or well [10], and could be misconstrued as indicating action at a distance if the influence of the pilot-wave field were not adequately resolved [5]. Moreover, long-range correlations between distant walkers may be established through the influence of the intervening wave field [21–23]. Recently, Papatryfonos *et al.* [24] and Frumkin *et al.* [25] established hydrodynamic analogs of superradiance, an effect originally attributed to quantum interference of two or more entangled atoms [26–28], but subsequently rationalized in terms of classical electromagnetic wave interference [29]. The accumulation of these results naturally raises the question as to whether this pilot-wave hydrodynamic system might exhibit bipartite correlations that violate Bell's inequality [30], and so provide a hydrodynamic analog of quantum entanglement, the acid test of quantumness. This question seems all the more pertinent given suggestions that Bell's Theorem may have no bearing on systems in which particles interact with a background field [30–32].

Bell's Theorem was derived by John Bell in 1964 [33] with a view to informing the Bohr-Einstein debate concerning the completeness of quantum theory [34]. Hidden variables are those variables that would be required for a complete description of quantum dynamics. For example, for the type of dynamics engendered in pilot-wave hydrodynamics, these would be the discrete variables defining the position and momentum of the particles, as well as the continuous variables defining the background field with which the particles interact. Quite generally, a Bell test can be performed on any physical system consisting of two subsystems (A and B) on which one measures a dichotomic property X (with stochastic outcomes of $+1$ or -1) that depends on some 'analyzer setting' (α or β). The measurement X_A made in the left two-level subsystem depends on the analyzer setting α which may take values a or a'; likewise, the measurement X_B made in the right two-level subsystem depends on β which may take values b or b'.

In the derivation of the Bell's inequality (Eq. (1), two assumptions are made. Assumption (i) is that the two subsystems undergo only local interactions. Specifically, X_A depends on α and not β; likewise, X_B depends on β and not α. Assumption (ii) is that the hidden variables that prescribe both X_A and X_B are independent of α and β. Bell's theorem [33] implies that for any classical system for which assumptions (i) and (ii) hold, the quantity $S(\alpha = a, \beta = b, \alpha = a', \beta = b') = M(a,b) + M(a',b) + M(a,b') - M(a',b')$ must satisfy the inequality

$$|S\left(a,b,a',b'\right)| \leq 2 \tag{1}$$

for any choice of measurement settings (a, a', b, b'). Here, $M(\alpha,\beta)$ is the average product,

$$M(\alpha,\beta) = \sum_{X_A,X_B} X_A X_B P(X_A, X_B|\alpha,\beta), \tag{2}$$

where $P(X_A, X_B|\alpha,\beta)$ is the joint probability of measurements (X_A, X_B) when the left and right analyzers are set, respectively, to $(\alpha,\ \beta)$. We note that Eq. (1) is cast in the form of the CHSH inequality [35]. It has been well established that quantum systems can violate the inequality (1) for a judicious choice of $(a,\ a',\ b,\ b')$, and these Bell violations are widely taken to be proof that the statistical behavior of quantum systems cannot be underlaid by a local, causal dynamics [36]. Quantum Bell tests were first performed with static analyzer settings [37], and so are referred to as static tests. In subsequent dynamic tests [38–44], the detector settings α and β were altered just prior to measurement, so that the two measurement events are space-like separated, so that assumption (i) is expected to hold true. Bell violations have been achieved with classical electro-

magnetic [45–48] and acoustic wave [49] systems. We here demonstrate the possibility of achieving Bell violations in a static test with a theoretical model of the walking-droplet system.

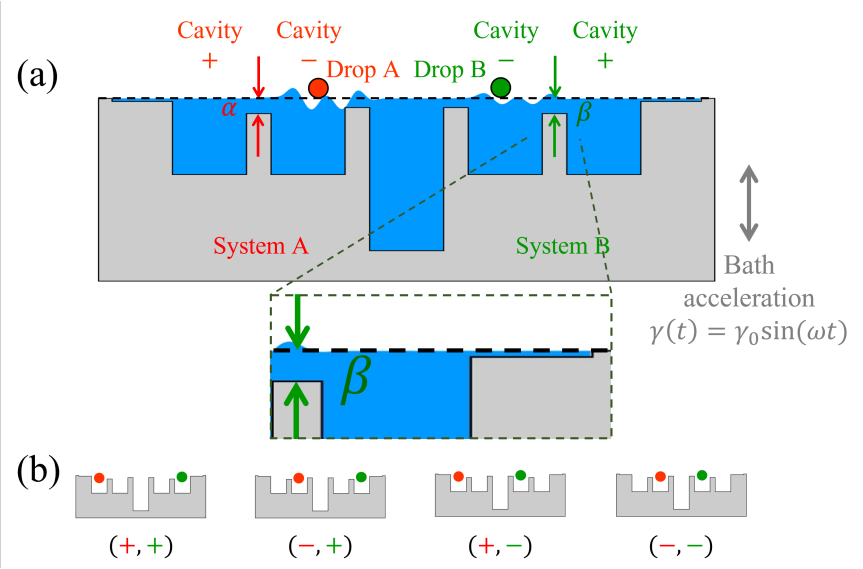

FIG. 1. **Hydrodynamic Bell test arrangement**. **(a)** Schematic of our hydrodynamic Bell test. The system consists of a pair of drops (red and green) walking on the surface of a vibrating liquid bath (blue) that spans the solid substrate (grey). Each drop is confined to its subsystem, a pair of wells separated by barriers across which they may tunnel unpredictably at a rate influenced by the barrier depths α and β, as may assume values of a, a' or b, b', respectively. (Inset) β is the distance between the unperturbed free surface and the top of the submerged pillar separating cavities (+) and (-) in subsystem B; α is analogously defined in subsystem A. **(b)** The four possibilities for the droplet configuration space, (X_A, X_B).

II. MODEL AND METHODS

We consider a pair of walking droplets in the bipartite tunneling system introduced by Papatryfonos *et al.* [24] in their demonstration of a hydrodynamic analog of quantum superradiance (See Fig. 1a). We describe this system in terms of two coupled, two-level systems, as shown schematically in Fig. 1b. The two subsystems, labelled A and B, contain a single, wave-generating particle confined to a pair of identical cavities separated by a barrier across which the particles may tunnel. The measurements X_A and X_B in our Bell experiment indicate whether the droplets are in the inner well ($X_j = -1,\ j = A,\ B$) or the outer well ($X_j = +1,\ j = A,\ B$) at the time of measurement. Each particle generates waves and moves in response to them according to equations (3)-(5). In each subsystem, the preferred cavity corresponds to the ground state ($-$) and the other

to the excited state (+). The ground state may be either the inner or outer cavity, depending on the geometry of the outer cavities [24]. For the specific geometry considered here, the inner cavity of each subsystem is the ground state (−); the outer cavity, the excited state (+) (see Fig. 1b). The two subsystems are separated by a coupling cavity of fixed length L_c, and by barriers that are sufficiently high as to preclude the particles from tunneling into the coupling cavity. Waves are transmitted across the central cavity, and so provide the coupling between subsystems A and B. The strength of this coupling is prescribed by the geometry of the central cavity: by increasing its depth d_c, the coupling may be increased, allowing the coupling cavity to serve as a nearly resonant transmission line [21]. Transitions between ground and excited states in the subsystems correspond to individual tunneling events, the rate of which depends on the depths of the submerged barrier, denoted α for the subsystem A and β for the subsystem B. These barrier depths α and β thus serve as the measurement settings in our Bell tests.

We employ the numerical simulation method developed by Nachbin [21, 50] for the one-dimensional motion of walking droplets over a vibrating liquid bath with complex topography. We adapt this model in order to consider the cooperative tunneling of two identical particles in the geometry depicted in Fig. 1a. Two identical particles of mass m are confined to their respective subsystem (A or B), and their positions, x_j ($j = A, B$), evolve according to Newton's Law:

$$m\ddot{x}_j + c\ F(t)\dot{x}_j = -F(t)\ \frac{\partial \eta}{\partial x}(x_j(t), t). \tag{3}$$

The particles move in response to gradients of the wave elevation $\eta(x, t)$. The waves are generated in a manner consistent with models of the vertical droplet dynamics [51, 52]. The droplet impacts the free surface with the Faraday frequency $\omega_F = \omega/2$ at a prescribed time relative to the vibrational forcing, making first contact when $\omega t = 0.45\pi$. Waves are generated during the contact time, of duration $T_c = T_F/4$, where $T_F = 2\pi/\omega_F$ is the Faraday period, a value consistent with laboratory experiments [51] and used in prior studies [50, 52]. During impact, the droplet is accelerated by the wave slope and decelerated by a drag force proportional to its horizontal speed, a drag coefficient $c = 0.01$ s/cm and the normal force imparted to the droplet by the interface, $F(t)$. The time dependence of these propulsive and drag forces is prescribed by $F(t) = (2\pi^2 mg)/(\omega T_c)\ \sin(\pi t/T_c)\ \mathbf{1}_{T_c}$, as follows from the linear-spring-like response of the interface in the walker system [50, 52, 53]. Here, g is the gravitational acceleration, and the periodic indicator function $\mathbf{1}_{T_c}$ highlights the intermittent nature of the forcing imparted by the interface to the bouncing droplets, which acts only during impact. By generating waves during impact, the droplets establish their own time-dependent wave potential, which serves as the memory of the system [15]. The wave forcing

enters the droplet trajectory equation through the final term in Eq. (3), and is computed as follows.

The velocity potential of the liquid bath $\phi(x, z, t)$ is a harmonic function satisfying Laplace's equation. In the bulk of the fluid, the velocity field is given by $(u, v) = \nabla\phi$. The wave model is formulated in the bath's vibrating reference frame, where the effective gravity is $g(t) = g+\gamma\sin(\omega t)$. The wave field thus evolves according to [50, 52]:

$$\frac{\partial\eta}{\partial t} = \frac{\partial\phi}{\partial z} + 2\nu\frac{\partial^2\eta}{\partial x^2}, \tag{4}$$

$$\frac{\partial\phi}{\partial t} = -g(t)\eta + \frac{\sigma}{\rho}\frac{\partial^2\eta}{\partial x^2} + 2\nu\frac{\partial^2\phi}{\partial x^2} - \sum_{j=A,B}\frac{\tilde{c}F(t)}{\rho\pi R^2}\mathbf{1}_{D_j}. \tag{5}$$

The particles ($j = A, B$) generate waves on the free surface by imparting, during impact, a pressure-like term over an area corresponding to the droplet's diameter, $D_j = 2R = 0.07$ cm, as denoted by the spatial indicator function $\mathbf{1}_{D_j}$. $\tilde{c} = 0.95$ is a dimensionless constant that prescribes the strength of the impact-induced wave forcing. Consistent with our modeling of the droplet dynamics, the wave forcing coefficient $F(t)$ is activated only during the contact time $T_c = T_F/4$. The forcing terms of this wave-particle dynamical system are discontinuous in both time and space, as highlighted by the indicator functions arising in Eqs. (3) and (5). Through the imposition of periodic wave-particle coupling at the Faraday frequency, we insure resonance between the particle and the most unstable Faraday mode of the bath [52], a key feature of pilot-wave hydrodynamics [4, 5, 54].

In equations (3)-(5), spatial derivatives are computed using the Fast Fourier Transform (FFT) in x. The shallow outer reaches of the fluid domain extend sufficiently far to ensure quiescent conditions in the far field. The vertical speed at the free surface $\phi_z(x, 0, t)$ is defined through a Dirichlet-to-Neumann (DtN) operator [50] and yields a Fourier integral operator computed in a straightforward fashion through an FFT. The DtN operator mathematically reduces the two-dimensional fluid problem to one spatial variable defined along the undisturbed free surface. To compute the DtN operator, a numerical conformal mapping is performed that maps the (x, z) fluid domain onto a (ξ, ζ) canonical flat strip. Details of the conformal mapping can be found elsewhere [55, 56]. The mapping for a given geometry is computed only once and provides the relation $x = x(\xi)$ along the undisturbed free surface. We denote by $\mathcal{F}$ the FFT in the ξ-coordinate, which runs along the undisturbed free surface in the canonical domain. We denote by $\phi(x, 0, t)) =$

$\varphi(x,t)$ the Dirichlet data. We thus have that

$$\phi_z(x,0,t) = DtN[\phi](x,t) = \frac{\mathcal{F}^{-1}[G(k)\mathcal{F}[\varphi(\xi)]]}{M(\xi(x,0))}, \tag{S1}$$

where $G(k) = k\tanh k$ is the Fourier multiplier [50]. The metric coefficient is $M(\xi) = \sqrt{|J|}$, where $|J|$ is the Jacobian of the $((x,z) \to (\xi,\zeta))$ change of variables, evaluated along the undisturbed free surface [55, 56]. To summarize, the geometrical information of the cavities and barriers is encoded in M and in $\xi = \xi(x,0)$, which is obtained with the inverse map. The time evolution is performed with a second-order fractional-step Verlet method [50].

System parameters are chosen to correspond to a fluid bath of density $\rho = 0.95$ g/cm^3, viscosity $\nu = 16$ cS and surface tension $\sigma = 20.9$ dynes/cm vibrating vertically in a sinusoidal fashion with peak acceleration $\gamma = A_0\omega^2$, peak amplitude A_0 and frequency $\omega/2\pi = 80$ Hz. The resonant bouncing of the particle at the Faraday frequency triggers a quasi-monochromatic damped wave pattern with a corresponding Faraday wavelength of $\lambda_F = 4.75$ mm. Each of the four cavities has a fixed length of 1.0 cm, corresponding to approximately $2.1\lambda_F$ and a fixed depth of 0.5 cm. The central cavity, coupling the right and left subsystems, has a fixed length of 0.4 cm and a fixed depth of 2 cm. Each of the barriers has a fixed width of 0.4 cm. The two barriers connecting the central cavity to the right and left sub-system, have a fixed depth of 0.045 cm. For this geometry, the critical vibrational acceleration above which waves are generated in the absence of the droplets, the Faraday threshold, was $\gamma_F = 4.69g$. We report results attained with a fixed vibrational acceleration $\gamma = A_0\omega^2 = 4.23g = 0.92\gamma_F$.

We proceed by demonstrating that for a judicious choice of pairs of static measurement settings (α,β), the inequality (1) may be violated in our bipartite hydrodynamic system owing to the wave-mediated coupling between the two subsystems. In our numerical simulations, each run begins by placing the two particles at random positions within their own subsystem. Their trajectories are then calculated for 48000 Faraday periods. During that time, we observe in which cavities the droplets reside. X_A takes the value -1 if the drop A is observed in the ground state of the left subsystem, and $+1$ otherwise. Similarly, X_B takes the value -1 if the drop B is observed in the ground state of the right subsystem, and $+1$ otherwise. The robustness of the emergent statistics was ensured by following the protocol detailed in Appendix A.

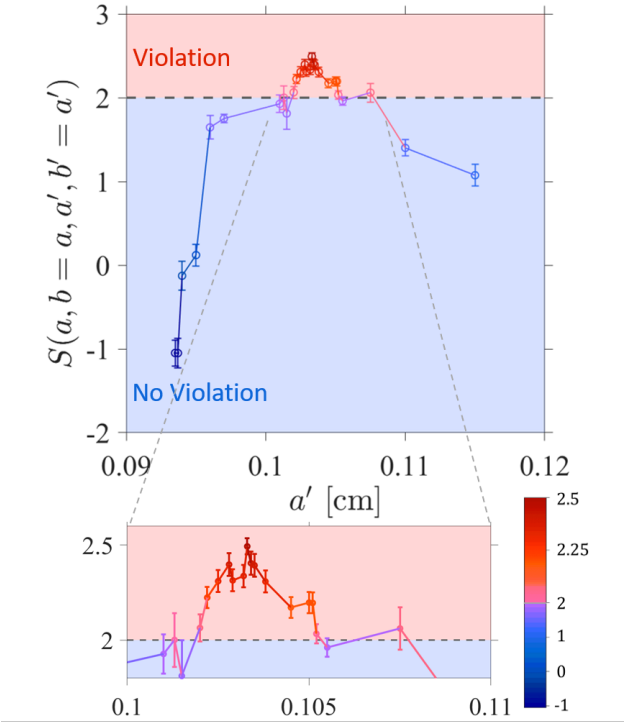

FIG. 2. **Violation of Bell's inequality**. Bell parameter $S(a, a, a', a')$ as a function of the barrier depth, a', for the symmetric case of $a = b$, $a' = b'$. For the calculation of the corresponding correlation functions, $M(a, a)$, $M(a, a')$ and $M(a', a')$, the barrier depth $a = a^* = 0.099$ cm remains fixed. For each combination of measurement settings, runs continue until statistics converge. The maximum Bell violation appears at $a'^* = 0.1033$cm, where $S = 2.49 \pm 0.04$.

III. RESULTS

Our main result is shown in Fig. 2, which indicates a narrow parameter range in which the CHSH inequality is violated. While the inequality can be violated in our system with four different values of the measurement settings (a, a', b, b'), our exploration of the (a, a', b, b') parameter-space indicates that a local maximum of S arises when $b = a$ and $b' = a'$, the symmetric case in which one may write $S(a, b, a', b') = S(a, a, a', a') = M(a, a) - M(a', a') + 2M(a, a')$. We deduced a maximum violation of $S_{\max} = 2.49 \pm 0.04$ when $a = b = a^* = 0.099$ cm and $a' = b' = a'^* = 0.1033$ cm. In Fig. 2, we plot S as a function of a' for fixed $a = a^*$, with the dashed line showing the limit $S = 2$ above which the CHSH inequality, Eq. (1), is violated.

While the inequality was found to be violated only for a narrow range of parameters settings, in this parameter regime, the violation is clear, and the statistical confidence of the violation is above 20 standard deviations (see Fig.6). We note that this behavior is reminiscent of the quantum case,

where, without guidance from the theory, it is relatively difficult to find analyzer settings that allow for violation of the CHSH inequality, but for judiciously chosen settings, the inequality is violated substantially. As in our previous study of superradiance [24], the wave-mediated coupling creates a collective behavior of the droplet pairs. In particular, when one of the droplets transitions to its excited state, the probability of the second droplet doing likewise increases substantially. Thus, through its wave-mediated interaction with its partner, each droplet is indirectly affected by the barrier depth of the distant station.

Since the inequality involves four different correlation functions (three for the symmetric case considered here), finding the combinations of measurement settings that maximized S was not entirely straightforward. The strategy we followed in seeking violations is summarised in Fig. 3. We first investigated the evolution of a single correlation function $M(\alpha = a, \beta = a)$ as a function of a. This gave us a good sense of parameters that maximize the difference $\delta M(a, a') = M(a, a) - M(a', a')$ (see Fig. 3a). $\delta M(a, a')$ involves two of the correlation functions of Eq. 1, in the symmetric case of interest where a=b and a'=b'. Figure 3b shows a 2D plot of the optimisation of δM as a function of a and a'. The black dashed lines highlight the domain in which $(\max_{a,a'}(\delta M) - \delta M)/\max_{a,a'}(\delta M) > 0.9$. The other term in the inequality, specifically $2M(\alpha = a, \beta = a')$, represents a combination of measurements from unequal barrier depths at the two measurement stations. Figure 3c represents the dependence of $2M(\alpha = a^*, \beta = a')$ on depth a' for fixed $a = a^*$, the S-maximizing value considered in Fig. 2. a'^* marks the end of the plateau of high correlation, beyond which the term $M(a^*, a')$ decreases. Finally, Fig. 3d shows the evolution of the correlation functions $(M(a, a'); M(a', a'))$ with increasing a' and fixed $a = a^*$.

The maximum S value occurs for moderate barrier depths, for which the droplets may become most strongly correlated through the background wave field. In Fig. 4a, we show typical trajectories for the three combinations of measurement settings $(\alpha, \beta) \in \{(a^*, a^*), (a^*, a'^*), (a'^*, a'^*)\}$ that maximize S. For $(a, a') = (a^*, a'^*)$, S is maximized because $M(a^*, a^*)$ and $M(a^*, a'^*)$ are large (see Fig. 4a top and middle panels), while $M(a'^*, a'^*)$ is relatively small (Fig. 4a lower panel). Figure 4b corresponds to a shallow barrier, $a' = 0.0937$ cm (the leftmost value in Fig. 2) and Fig. 4c to a relatively deep barrier, $a' = 0.11$ cm (the right-most value in Fig. 2). Figures 4b and c correspond to minima of S occurring when the a' barrier is either too shallow (Fig. 4b) or too deep (Fig. 4c).

The degree of synchronization in the droplet tunneling depends on the extent to which the droplets are affected by the barrier depth in the distant station. When the barrier depth in one station is too small, the local particle is prevented from tunneling, regardless of the barrier depth

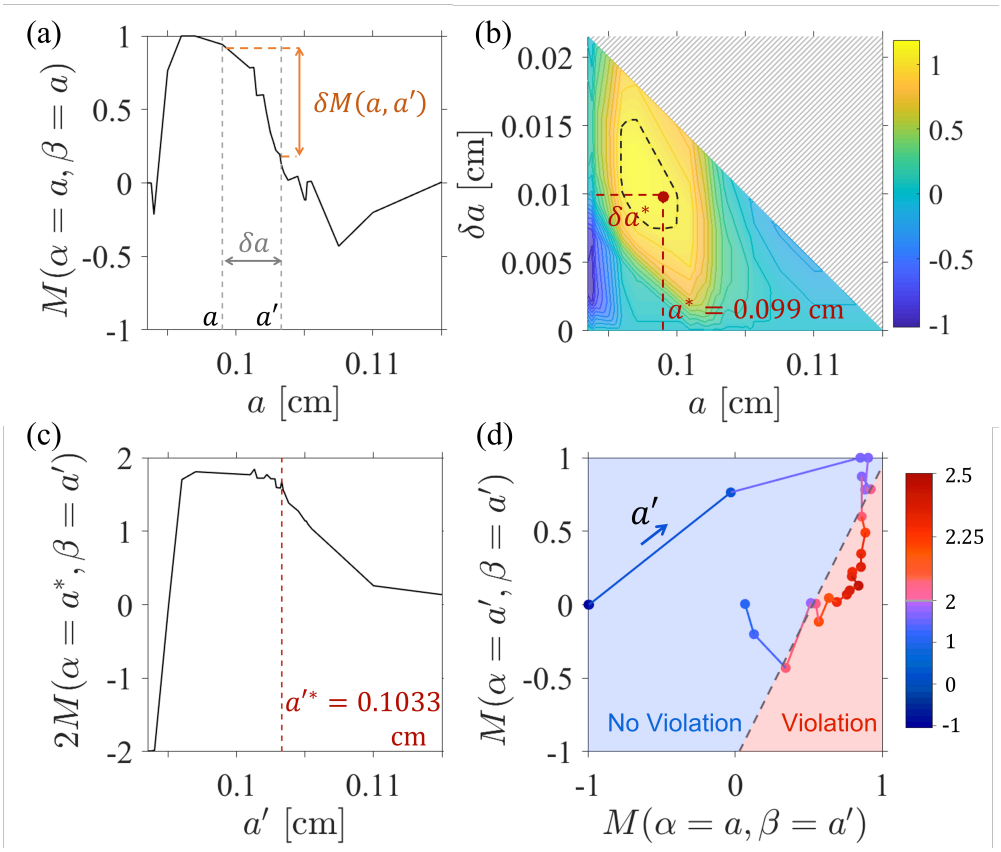

FIG. 3. **Strategy to optimize $S(a, a, a', a') = M(\alpha = a, \beta = a) - M(\alpha = a', \beta = a') + 2M(\alpha = a, \beta = a')$** . S is optimized by searching a parameter regime (a, a') near the maximum of $\delta M(a, a') = M(\alpha = a, \beta = a) - M(\alpha = a', \beta = a')$ and a range of a' that maximizes $M(a, a')$ with a fixed. **(a)** Evolution of $M(\alpha = a, \beta = a)$ as a function of a. The indicated values $a^* = 0.099$ cm and $a'^* = 0.1033$ cm are the S-maximizing values used in Figs 2. We note $\delta a = a' - a$ and $\delta a^* = a'^* - a^*$. The difference between the corresponding correlation functions $\delta M(a, a + \delta a) = \delta M(a, a') = M(\alpha = a, \beta = a) - M(\alpha = a', \beta = a')$ is marked in orange. **(b)** Optimization of $\delta M(\alpha = a, \beta = a + \delta a)$ as a function of barrier depth a and δa. The domain for which $(\max_{a,a'}(\delta M) - \delta M)/\max_{a,a'}(\delta M) > 0.9$ is bound by the black dashed curve. **(c)** $2M(\alpha = a^*, \beta = a')$ as a function of depth a' for fixed $a = a^*$. **(d)** Evolution of $S(a, a, a', a')$ in the correlation representation space $(M(a, a'); M(a', a'))$ with $a = a^*$. The direction of increasing a' is indicated by the blue arrow. The dots are colored with respect to their S values. The grey dashed line indicates the limiting case of $S = 2$.

in the other. The synchronization of states is thus reduced substantially. Conversely, when the barrier depth is too large, the particle generally tunnels across it, unaffected by the distant particle. Thus, the synchronization again remains relatively low. For intermediate barrier depths, each particle tunnels with a moderate probability that is strongly affected by the behavior of its distant partner.

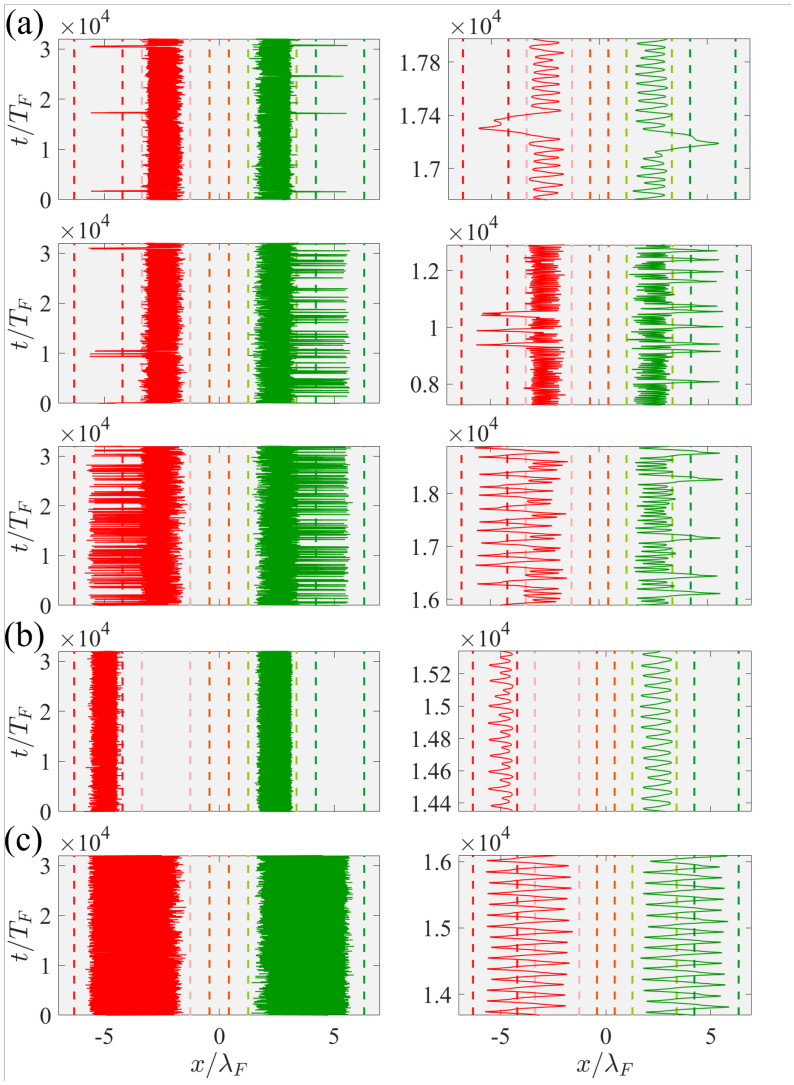

FIG. 4. **Trajectory analysis**. **(a)-(c)** Droplet trajectories for the symmetric case $(\alpha,\beta) \in (a, a')$ with $a = a^* = 0.099$ cm. Time evolves in the vertical direction. In **(a)**, $a' = a'^*$=0.1033 cm (the maximizing value for S); in **(b)**, $a' = 0.0937$ cm; in **(c)**, $a' = 0.11$ cm. **(a)** Trajectories corresponding to the three correlation functions $M(a^*, a^*) = 0.94$ (upper panel), $M(a^*, a'^*) = 0.84$ (middle panel), and $M(a'^*, a'^*) = 0.13$ (lower panel). The tunneling events are highly correlated only in the upper and lower panels. **(b)** Trajectories corresponding to $M(a^*, a')$ with $a' = 0.0937$ cm. When the barrier depth a' is sufficiently small, the wave-mediated communication between droplets is diminished, and droplets tend to get trapped in one cavity, leading to minima of S and $M(a^*, a') \approx 0$ when we average over the droplet's initial conditions. **(c)** Another minimum of $M(a^*, a')$ and S occurs when one of the barrier depths is too large, in which case one of the droplets tunnels continuously, unimpeded by the barrier, as if it were in a single cavity. Averaging over all initial conditions leads to a relatively low value of $M(a^*, a') \approx 0$. Note that the correlation function is deduced by averaging over all initial conditions in both subsystems.

Finally, to ensure that the dynamics were a result of the two-droplet state rather than just the topography, we ran several complementary single-drop simulations with the same topographies. A typical example is presented in Figure 5, where we compare the two extreme cases, one in which the distant barrier depth is relatively low (b=0.099 cm) and another in which it is relatively high (b'=0.1033 cm). In these simulations we set a=0.099 cm, so the overall topography was identical to that reported in Figure 4a for a pair of drops. We observe that the single-drop trajectories in the two cases are identical for these values of b and b', but substantially different from those arising in the two-particle case. Thus, when only one drop is present, the variation of the measurement setting in the distant subsystem does not influence its behavior. This indicates that, in the two-droplet case, the droplets learn about the distant cavity geometry (or 'measurement setting') only through their wave-mediated interactions with their partner drop. This result is consistent with previous findings on superradiance [24], where for certain topographies the single-droplet tunneling rate was very low, unless a second drop was introduced into the distant cavity, in which case the tunneling probabilities could increase dramatically.

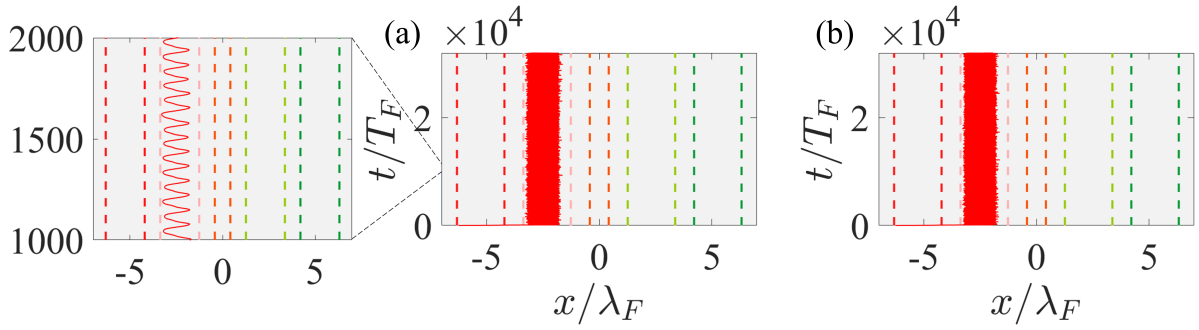

FIG. 5. **Single drop trajectory analysis**. **(a)** Single droplet trajectory for a relatively shallow distant barrier: a=0.099 cm; b=0.099 cm. Inset: a close-up of the dynamics illustrates the oscillatory motion of the drop inside the cavity (-). **(b)** Single droplet trajectory for a relatively deep distant barrier: a=0.099 cm; b'=0.1033 cm. The two trajectories are statistically indistinguishable, indicating that, in the absence of a partner drop, the droplet motion is not influenced by the distant barrier depth.

IV. CONCLUSION AND DISCUSSION

We have devised a platform for performing static Bell tests on a classical bipartite pilot-wave system. The maximum violation was found to be 2.49 ± 0.04, and arose when the system ge-

ometries were chosen such that the droplet motion was marked by varying degrees of correlation between droplets with different measurement settings. A key step in the process was recognizing that the system geometry may serve as a proxy for analyzer settings in the quantum Bell tests. The non-Markovian nature of the droplet dynamics is engendered in the system memory [15], the critical feature in all hydrodynamic quantum analogs [5]. The wave field serves as the memory of the system, and the correlations reported here may be understood as being rooted in this wave-mediated memory. We have focused here on the intermediate memory regime ($\gamma/\gamma_F = 0.92$, where the wave-mediated interactions allow for Bell violations. We note that these violations vanish at much lower memory, when there is insufficient wave-coupling between the two subsystems, and at higher memory, when the droplet dynamics becomes highly disordered.

We proceed by rationalizing the Bell violation achieved in our static test. Specifically, we identify which of the assumptions made in the derivation of Bell's inequality are not applicable in our system. In order to do so, we find it valuable to adopt two distinct perspectives in the form of two fictional observers. Observer 1 can observe the droplets but not the waves, while Observer 2 can observe both droplets and waves. Observer 1 would infer that the measurements at each subsystem are influenced by the distant measurement setting, and thus that assumption (i) is invalid. Through consideration of the wave field, Observer 2 could rationalize the violation of assumption (i) in terms of the wave-mediated coupling between the two subsystems. It would also be apparent to Observer 2 that the wave field constituting the continuous variable hidden from Observer 1 is affected by both analyzer settings. Observer 2 would thus conclude that both assumptions (i) and (ii) are invalid.

Quantum entanglement requires that the violations of Bell's inequality persist even when the two subsytems are space-like separated. While such entanglement is generally thought to be peculiar to quantum systems, Bell-violating states have been demonstrated in both classical electromagnetic [45–47] and acoustic wave systems [49]. They have also been reported in single-particle systems, through consideration of the internal degrees of freedom of a single neutron [57]. However, neither the classical wave states nor the internal degrees of freedom in the single-particle system can be spatially separated [48, 58]. We have here demonstrated the possibility of achieving static Bell violations for spatially separated bipartite states in the pilot-wave hydrodynamic system. We stress that these violations may be simply rationalized: the wave-mediated coupling between the two subsystems ensures that both the assumptions (i) and (ii) made in the derivation of Bell's

inequality are invalid. Nevertheless, the violations exist only in a limited region of parameter space, and so are relatively difficult to achieve.

Finally, we note that our theoretical framework introduces the possibility of performing more sophisticated Bell tests. The feasibility of incorporating time-dependent topography into our model has recently been demonstrated by Nachbin [22], who demonstrated the persistence of correlations between droplet pairs in single wells even after their topographic isolation. Incorporating dynamic topography will allow for future Bell tests in which communication between the two subsystems is eliminated by closing the coupling cavity during the course of a simulation. The dynamic-Bell-test protocol would then involve changing the analyzer settings after topographic isolation of the two subsystems. However unlikely, attaining Bell violations in such dynamic tests does not seem entirely impossible given that the wave field serves as the memory of the system; thus, the mutual memory of the initial wave-mediated droplet interaction might survive the topographic isolation of the two subsystems.

V. ACKNOWLEDGEMENTS

The code and the data that generated the data are available upon request. We acknowledge the generous financial support of the NSF through grants CMMI-1727565 and CMMI-2154151, the European Union's Horizon 2020 Research and Innovation Program under the Marie Sklodowska-Curie project EnHydro, grant No. 841417, and the CNPq under (PQ1D) 307078/2021-3 and FAPERJ CNE, Project No. E-26/201.156/2021.

APPENDIX A: STATISTICAL CONVERGENCE

To confirm the statistical significance of our results, we performed 6 runs with durations of 48000 Faraday periods for each geometrical configuration. We used random initial conditions for the particle positions, and discarded the first 10% of the runs in order to eliminate any trace of a transient. To initialize the runs, the wave and velocity fields of the bath are set to zero, and the particle positions are assigned random, uniformly distributed values. Then, the model runs for 2000 Faraday periods, a measurement is made, and all fields are reset back to zero to initialize the subsequent run. This cycle is repeated for each set of parameter settings until the relative error in the running average of $M(\alpha = a, \beta = b)$ is reduced to an acceptably small value. We set this

tolerance to be 3% for parameters that violate the inequality and 7% for those that do not. While extremely accurate, this 'discrete' technique is computationally intensive; thus we have used it only for the most critical points of the parameter space, in which the maximal Bell violations occurred.

To explore the parameter space more efficiently, we adopt an alternative, relatively expedient, 'continuous' approach, in which the final conditions of one run serve as the initial conditions of the next. We demonstrated the statistical equivalence of the two approaches as follows. For specific selected data points, we performed approximately 30 different runs using the two techniques, and found the results of the 'discrete' and 'continuous' runs to be in agreement to within 3%. We then executed continuous runs for 48,000 Faraday periods, during which measurements are performed frequently at uniformly distributed random times. After a sufficiently long run, the full range of initial conditions will have been effectively explored. The consistency of the results deduced with the discrete and continuous approaches demonstrates that the long-time emergent statistics are independent of the initial conditions. Figures 6a and 6b show a typical example of the convergence of the 'running average' with the number of runs which determines the relative error of our statistics. This approach indicates when our statistics have converged for each $M(\alpha, \beta)$ calculation, specifically when the relative error has fallen below the prescribed tolerance.

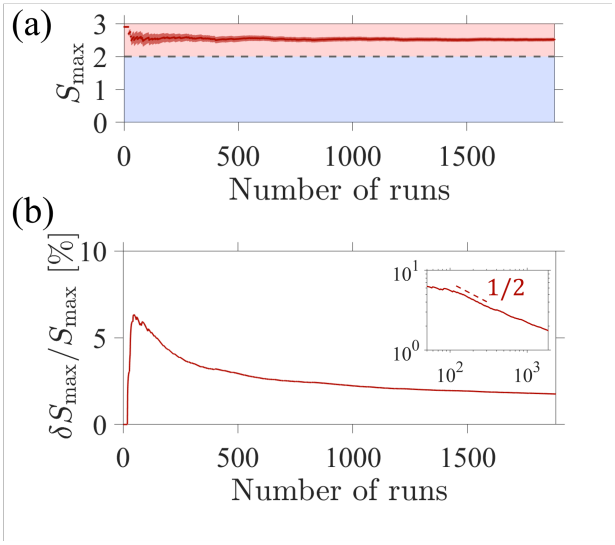

FIG. 6. **Statistical convergence of the Bell parameter**. **(a)** Typical curve showing the convergence of $S_{\max}$, the Bell parameter taken at the maximum point of violation ($a = b = a^* = 0.099$ cm; $a' = b' = a'^* = 0.1033$ cm). The error bars indicate ± 3 standard deviations. **(b)** Relative error $\delta S_{\max}/S_{\max}$ of the estimation of the Bell parameter S with the number of runs, evaluated for the maximum point of violation ($a = b = a^*; a' = b' = a'^*$). Inset: log-log scale; the dashed line indicates a $-1/2$ slope as expected from the convergence of an ensemble average.

[1] Y. Couder, S. Protière, E. Fort, and A. Boudaoud. Walking and orbiting droplets. *Nature*, 437(208), 2005.

[2] Y. Couder and E. Fort. Single particle diffraction and interference at a macroscopic scale. *Phys. Rev. Lett.*, 97(154101), 2006.

[3] E. Fort, A. Eddi, J. Moukhtar, A. Boudaoud, and Y. Couder. Path-memory induced quantization of classical orbits. *Proc. Natl. Acad. Sci.*, 107(41):17515–17520, 2010.

[4] J. W. M. Bush. Pilot-wave hydrodynamics. *Ann. Rev. Fluid Mech.*, 47, 2015.

[5] J. W. M. Bush and A. U. Oza. Hydrodynamic quantum analogs. *Reports on Progress in Physics*, 84(1):017001, 2020.

[6] G. Pucci, D. M. Harris, L. M. Faria, and J. W. M. Bush. Walking droplets interacting with single and double slits. *J. Fluid Mech.*, 835:1136–1156, 2018.

[7] C. Ellegaard and M. T. Levinsen. Interaction of wave-driven particles with slit structures. *Phys. Rev. E*, 102:023115, Aug 2020.

[8] S. Perrard, M. Labousse, M. Miskin, E. Fort, and Y. Couder. Self-organization into quantized eigenstates of a classical wave-driven particle. *Nat. Commun.*, 5(3219), 2014.

[9] A. Eddi, E. Fort, F. Moisy, and Y. Couder. Unpredictable tunneling of a classical wave-particle association. *Phys. Rev. Lett.*, 102(240401), 2009.

[10] P. J. Sáenz, T. Cristea-Platon, and J. W. M. Bush. A hydrodynamic analog of Friedel oscillations. *Science Advances*, 6(20), 2020.

[11] V. Frumkin, D. Darrow, W. Struyve, and J. W. M. Bush. Real surreal trajectories in pilot-wave hydrodynamics. *Physical Review A*, 106(L010203), 2022.

[12] P. J. Sáenz, G. Pucci, S. E. Turton, A. Goujon, R. R. Rosales, J. Dunkel, and J. W. M. Bush. Emergent order in hydrodynamic spin lattices. *Nature*, 596(7870):58–62, August 2021.

[13] D. M. Harris, J. Moukhtar, E. Fort, Y. Couder, and J. W. M. Bush. Wavelike statistics from pilot-wave dynamics in a circular corral. *Phys. Rev. E*, 88(011001):1–5, 2013.

[14] P. J. Sáenz, G. Pucci, A. Goujon, T. Cristea-Platon, J. Dunkel, and J. W. M. Bush. Spin lattices of walking droplets. *Phys. Rev. Fluids*, 3(100508), 2018.

[15] A. Eddi, E. Sultan, J. Moukhtar, E. Fort, M. Rossi, and Y. Couder. Information stored in Faraday waves: the origin of a path memory. *J. Fluid Mech.*, 674:433–463, 2011.

[16] P. Le Gal, B. Castillo Morales, S. Hernandez-Zapata, and G. Ruiz Chavarria. Swimming of a ludion in a stratified sea. *Journal of Fluid Mechanics*, 931:A14, 2022.

[17] A. Roux, J.-P. Martischang, and M. Baudoin. Self-radiation force on a moving monopolar source. *Journal of Fluid Mechanics*, 952:A22, 2022.

[18] G. P. Benham, O. Devauchelle, S. W. Morris, and J. A. Neufeld. Gunwale bobbing. *Phys. Rev. Fluids*, 7:074804, Jul 2022.

[19] I. Ho, G. Pucci, A. U. Oza, and D. M. Harris. Capillary surfers: Wave-driven particles at a vibrating fluid interface. *Phys. Rev. Fluids*, 8:L112001, Nov 2023.

[20] D. M. Harris, P.-T. Brun, A. Damiano, L. Faria, and J. W. M. Bush. The interaction of a walking droplet and a submerged pillar: From scattering to the logarithmic spiral. *Chaos*, 28(096106), 2018.

[21] A. Nachbin. Walking droplets correlated at a distance. *Chaos*, 28(096110), 2018.

[22] A. Nachbin. Effect of isolation on two-particle correlations in pilot-wave hydrodynamics. *Physical Review Fluids*, 7(9):093604, September 2022.

[23] R. N. Valani, A. C. Slim, and T. Simula. Hong–Ou–Mandel-like two-droplet correlations. *Chaos*, 28(9):096104, September 2018.

[24] K. Papatryfonos, M. Ruelle, C. Bourdiol, A. Nachbin, J. W. M. Bush, and M. Labousse. Hydrodynamic superradiance in wave-mediated cooperative tunneling. *Communications Physics*, 5:142, 2022.

[25] V. Frumkin, K. Papatryfonos, and J. W. M. Bush. Superradiant droplet emission from parametrically excited cavities. *Phys. Rev. Lett.*, 130:064002, 2023.

[26] R. G. DeVoe and R.G. Brewer. Observation of superradiant and subradiant spontaneous emission of two trapped ions. *Phys. Rev. Lett.*, 76:2049–2052, Mar 1996.

[27] A. A. Makarov and V. S. Letokhov. Metastable entangled states of atomic systems in macroscale: radiation dynamics and spectrum. *International Workshop on Quantum Optics 2003 (Proceedings of the SPIE)*, pages 54–64, 2004. Publisher: SPIE.

[28] A. Karnieli, N. Rivera, A. Arie, and I. Kaminer. Superradiance and subradiance due to quantum interference of entangled free electrons. *Phys. Rev. Lett.*, 127:060403, Aug 2021.

[29] H. Tanji-Suzuki, I. D. Leroux, M. H. Schleier-Smith, M. Cetina, A. T. Grier, J. Simon, and V. Vuletić. Chapter 4 - interaction between atomic ensembles and optical resonators: Classical description. In E. Arimondo, P.R. Berman, and C.C. Lin, editors, *Advances in Atomic, Molecular, and Optical Physics*, volume 60 of *Advances In Atomic, Molecular, and Optical Physics*, pages 201–237. Academic Press, 2011.

[30] L. Vervoort. Are hidden-variable theories for pilot-wave systems possible? *Foundations of Physics*, 48:803–826, 2018.

[31] P. Morgan. Bell inequalities for random fields. *J. Phys. A*, 39:7441–7455, 2006.

[32] L. De la Peña, A. M. Cetto, and A. Valdés-Hernández. The emerging quantum. *The Physics behind Quantum Mechanics. Cham: Springer International Publishing*, 2015.

[33] J. S. Bell. On the Einstein Podolsky Rosen paradox. *Physics*, 1(3):195–200, 1964.

[34] A. Einstein, B. Podolsky, and N. Rosen. Can quantum-mechanical description of physical reality be considered complete? *Physical Review*, 47(777), 1935.

[35] J. F. Clauser, M. A. Horne, A. Shimony, and R. A. Holt. Proposed experiment to test local hidden-variable theories. *Phys. Rev. Lett.*, 23:880–4, 1969.

[36] T. Maudlin. What Bell did. *Journal of Physics A: Mathematical and Theoretical*, 47:424010, 2014.

[37] A. Aspect, P. Grangier, and G. Roger. Experimental realization of Einstein-Podolsky-Rosen-Bohm

gedankenexperiment: A new violation of Bell's inequalities. *Phys. Rev. Lett.*, 49(91), 1982.

[38] A. Aspect, J. Dalibard, and G. Roger. Experimental test of Bell's inequalities using time-varying analyzers. *Phys. Rev. Lett.*, 49(1804), 1982.

[39] G. Weihs, T. Jennewein, C. Simon, H. Weinfurter, and A. Zeilinger. Violation of Bell's inequality under strict einstein locality conditions. *Phys. Rev. Lett.*, 81:5039–5043, Dec 1998.

[40] T. Scheidl, R. Ursin, J. Kofler, S. Ramelow, X. Ma, T. Herbst, L. Ratschbacher, A. Fedrizzi, N. K. Langford, T. Jennewein, , and A. Zeilinger. Violation of local realism with freedom of choice. *PNAS*, 107:19708–19713, 2010.

[41] B. Hensen, H. Bernien, A. Dréau, A. Reiserer, N. Kalb, M. S. Blok, J. Ruitenberg, R. F. L. Vermeulen, R. N. Schouten, C. Abellán, W. Amaya, V. Pruneri, M. W. Mitchell, M. Markham, D. J. Twitchen, D. Elkouss, S. Wehner, T. H. Taminiau, and R. Hanson. Loophole-free Bell inequality violation using electron spins separated by 1.3 kilometres. *Nature*, 526:682–686, 2015.

[42] N. Brunner, D. Cavalcanti, S. Pironio, V. Scarani, and S. Wehner. Bell nonlocality. *Rev. Mod. Phys.*, 86:419–478, Apr 2014.

[43] W. Tittel, J. Brendel, H. Zbinden, and N. Gisin. Violation of Bell inequalities by photons more than 10 km apart. *Phys. Rev. Lett.*, 81:3563–3566, Oct 1998.

[44] M. Giustina, M. A. M. Versteegh, S. Wengerowsky, J. Handsteiner, A. Hochrainer, K. Phelan, F. Steinlechner, J. Kofler, J.-A. Larsson, C. Abellán, W. Amaya, V. Pruneri, M. W. Mitchell, J. Beyer, T. Gerrits, A. E. Lita, L. K. Shalm, S. W. Nam, T. Scheidl, R. Ursin, B. Wittmann, and A. Zeilinger. Significant-loophole-free test of Bell's theorem with entangled photons. *Phys. Rev. Lett.*, 115:250401, Dec 2015.

[45] M. A. Goldin, D. Francisco, and S. Ledesma. Simulating Bell inequality violations with classical optics encoded qubits. *J. Opt. Soc. Am. B*, 27:779, 2010.

[46] X. Qian, B. Little, J. C. Howell, and J. H. Eberly. Shifting the quantum-classical boundary: theory and experiment for statistically classical optical fields. *Optica*, 2(7):611–615, Jul 2015.

[47] X. Song, Y. Sun, P. Li, H. Qin, and X. Zhang. Bell's measure and implementing quantum fourier transform with orbital angular momentum of classical light. *Sci Rep*, 5:14113, 2015.

[48] R. J. C. Spreeuw. A Classical Analogy of Entanglement. *Foundations of Physics*, 28(3):361–374, March 1998.

[49] M. Arif Hasan, L. Calderin, T. Lata, P. Lucas, K. Runge, and P. A. Deymier. The sound of Bell states. *Communications Physics*, 2(1):106, September 2019.

[50] A. Nachbin, P. A. Milewski, and J. W. M. Bush. Tunneling with a hydrodynamic pilot-wave model. *Physical Review Fluids*, 2(034801), 2017.

[51] J. Moláček and J. W. M. Bush. Drops walking on a vibrating bath: towards a hydrodynamic pilot-wave theory. *J. Fluid Mech.*, 727:612–647, 2013.

[52] P. Milewski, C. Galeano-Rios, A. Nachbin, and J. W. M. Bush. Faraday pilot-wave dynamics: modelling and computation. *J. Fluid Mech.*, 778:361–388, 2015.

[53] T. Gilet and J. W. M. Bush. The fluid trampoline: droplets bouncing on a soap film. *J. Fluid Mech.*, 625:167–203, 2009.

[54] S. Protière, A. Boudaoud, and Y. Couder. Particle-wave association on a fluid interface. *J. Fluid. Mech.*, 554:85–108, 2006.

[55] A. Nachbin. A terrain-following boussinesq system. *SIAM Journal on Applied Mathematics*, 63(3):905–922, 2003.

[56] A. S. Fokas and A. Nachbin. Water waves over a variable bottom: a non-local formulation and conformal mappings. *Journal of Fluid Mechanics*, 695:288–309, 2012.

[57] Y. Hasegawa, R. Loidl, G. Badurek, M. Baron, and H. Rauch. Violation of a Bell-like inequality in single-neutron interferometry. *Nature*, 425:45–48, 2003.

[58] E. Karimi and R. W. Boyd. Classical entanglement? *Science*, 350(6265):1172–1173, December 2015.